

Silver Nanowires on Carbon Nanotube Aerogel Sheets for Flexible, Transparent Electrodes

Patricia M. Martinez^{1, 2}, *Arthur Ishteev*^{3, 4}, *Josef Velten*¹, *Azin Fahimi*^{†, 5}, *Izabela Jurewicz*⁵,
*Alan B. Dalton*⁶, *Ray H. Baughman*^{1, 2} and *Anvar A. Zakhidov*^{*, 1, 3, 4}

¹ University of Texas at Dallas, NanoTech Institute, Richardson, TX, 75080, United States.

² University of Texas at Dallas, Department of Chemistry, Richardson, TX 75080, United states.

³ National University of Science and Technology, MISiS, Leninskiy prospect, Moscow, 119049,
Russia.

⁴ ITMO University, 49 Kronverksky Pr. St. Petersburg, 197101, Russia.

⁵ University of Surrey, Guildford, Surrey GU2 7XH, United Kingdom.

⁶ University of Sussex, Falmer, Brighton BN1 9RH, United Kingdom.

KEYWORDS: Silver nanowires, multiwall carbon nanotubes, percolation, conductive, transparent electrode, free-standing electrode.

ABSTRACT: Flexible, free-standing transparent conducting electrodes (TCEs) with simultaneously tunable transmittances up to 98% and sheet resistances down to 11 Ω /sq were prepared by a facile spray-coating method of silver nanowires (AgNWs) onto dry-spun multiwall

carbon nanotube (MWNT) aerogels. Counterintuitively, the transmittance of the hybrid electrodes can be increased as the mass density of AgNWs within the MWNT aerogels increase, however, the final achievable transmittance depends on the initial transparency of the MWNT aerogels. At the same time, a strong decrease in sheet resistance is obtained when AgNWs form a percolated network along the MWNT aerogel. Additionally, anisotropic reduction in sheet resistance and polarized transmittance of AgNWs/MWNTs aerogel is achieved with this method. The final AgNWs/MWNTs hybrid TCEs transmittance and sheet resistance can be fine-tuned by spray-coating mechanisms or by the choice of initial MWNT aerogel density. Thus, a wide range of AgNWs/MWNTs hybrid TCEs with optimized optoelectronic properties can be achieved depending of the requirements needed. Finally, the free-standing AgNWs/MWNTs hybrid TCEs can be laminated onto a wide range of substrates without the need of a bonding aid.

1. Introduction

The need to find materials for replacing Indium Tin Oxide (ITO) in flexible Transparent Conducting Electrodes (TCEs) has stimulated the search for low-cost, lightweight alternatives that have highly transparency and electrical conductivity, high mechanical strength, and compatibility with the numerous substrates used for optoelectronic devices. Though ITO combines high optical transmittance (>90% at 550 nm) with low sheet resistance ($10 \Omega/\text{sq}$)¹, applications of ITO-based flexible electrodes are limited by the scarcity of indium and the inherent brittleness of metal oxides^{2,3}. Novel technologies, such as for ITO nanowires⁴ and ITO mesh structures prepared via photolithography⁵, have been developed to prevent ITO from cracking. However, the fabrication of such flexible ITO TCEs requires complex processes that are expensive^{1,4}. Efforts have been made to develop flexible TCEs based on multi-walled carbon nanotubes (MWNTs)⁶⁻⁸, single-walled carbon nanotubes^{6,9-16}, graphene¹⁷⁻²⁰, and a combination

of the above^{3,21–23} as alternatives to ITO⁶. Of particular interest are free-standing MWNT aerogels sheets that can be drawn in the dry state from the side of spinnable MWNT forests²⁴. These highly oriented aerogels sheets are porous, transparent, flexible, and conducting. When contacted with organic solvents, such as isopropyl alcohol (IPA) or methanol, they densify during solvent evaporation, reducing sheet thickness from ~20 μm to ~50 nm. MWNT aerogels can also be laminated to a wide range of substrates by contacting the desired section with an organic solvent and allowing surface tension effects during evaporation to densify the aerogel, increasing the contact area between MWNTs and the substrate²⁴. However, these self-supported aerogels are highly electronically and optically anisotropic, which can be an undesired property for optoelectronic devices.

Though the use of carbon-based nanomaterials improves the flexibility of TCEs, their low conductivity and transmittance limits optoelectronic performance²⁵. Their comparatively high sheet resistances and low transmittances make them unsuitable choices when the need is an optical transmittance above 90% and a sheet resistance below 100 Ω/sq ^{26,27}. Thus, substantial optical and electrical improvements are necessary for carbon-based nanomaterials to become viable TCEs alternatives.

By integrating silver nanowires (AgNWs) with carbon-based nanomaterials, hybrid TCEs having low sheet resistances and high transmittances, similar to ITO, can be realized^{28,29}. The optical and electrical properties of these hybrid TCEs improve when AgNWs percolation networks are formed, increasing the number of conduction pathways connecting AgNWs either to themselves or to the carbon nanomaterial^{27,30,31}. These hybrid TCEs provide direct proportionality between sheet resistance and transmittance, as the amount of AgNWs deposited defines the maximum sheet resistance that can be obtained without losing transparency of the

substrate²⁷. Previous studies have shown that AgNWs can be easily combined with carbon nanomaterials by spray-coating, spin coating, drop-casting, or roll-coating to form hybrid TCEs^{3,17,37-45,18,19,21,32-36}. From these techniques, spray-coating is the most suitable and scalable technique since it can be used over large volumes with high reproducibility, while insuring homogeneous AgNW distributions^{31,46}.

Typically, AgNWs-carbon hybrid TCEs deploy polyethylene terephthalate (PET)⁴⁷⁻⁵⁰, polyethylene naphthalate (PEN)⁵¹, or polydimethylsiloxane (PDMS)⁵² as the flexible substrate and receive a post-treatment to further optimize the transmittance and sheet resistance. Post-treatments ranging from thermal annealing^{53,54}, mechanical pressing⁵⁵, photophysical welding^{56,57}, low energy plasma⁵⁸, or electrochemical Ostwald ripening processes⁵⁹ are quite successful, but require fabricating the hybrid electrodes separated from the optoelectronic devices to prevent damage of the layers. Free-standing TCEs that can be laminated onto any device layer have been developed for single-component-based materials, such as metallic AgNWs networks⁶⁰, graphene films⁶¹, single-walled carbon nanotubes⁶² or MWNT aerogels²⁴. In contrast, most of the reported hybrid carbon/metal TCEs are substrate-supported. Hence, it would be valuable to fabricate free-standing AgNWs-carbon based hybrids that meet industrial requirements for TCEs and could be laminated onto any substrate surface.

In this work, free-standing carbon/metal hybrid TCEs are produced in which the optical, electrical and mechanical properties of dry-spun MWNT aerogels are combined with the attributes of AgNWs. To avoid the trade-off between transmittance and sheet resistance, free-standing MWNT aerogels are spray-coated with a solution of AgNWs in IPA. This results in simultaneous increase in transmittance and decrease in sheet resistance as the density of AgNWs increases within the MWNT aerogel. Taking advantage of MWNT aerogel densification by

evaporating organic solvents, apertures greater than the wavelength of light form in the aerogel, which increases overall transmittance. Also, relying on the high thermal conductivity of MWNT aerogels⁶³, the contact resistance of the AgNWs is reduced when a fast 1-2 minute thermal annealing process is performed. As a result, free-standing AgNWs/MWNTs hybrids with sheet resistances $\sim 11 \Omega/\text{sq}$ and transmittances $\sim 98\%$ are produced that can be laminated onto targeted substrates. Thus, the described technology produces AgNWs/MWNTs hybrid TCEs that exceed industrial requirements for TCEs in optoelectronic devices.

2. Experimental Section

2.1. Materials. Two types of AgNWs suspensions, AgNW-25 and AgNWs-60 with concentrations of 5mg/mL in isopropyl alcohol (IPA) were purchased from Seashell Technologies. The mean lengths were 30 μm and 15 μm , with mean diameter of 25 nm and 60 nm, respectively. The AgNWs solution was diluted to a concentration of 0.25 mg/ml with IPA prior to spray coating. AgNWs with diameters between 50-150 nm and lengths greater than 20 μm were synthesized by a polyol method, described by Vinogradov et al⁶⁴.

2.2. Silver evaporation. A 10 nm thick layer of silver was evaporated onto MWNT aerogels with a CHA-50 electron beam evaporator at a rate of 1.2-1.7 A/sec. Prior to Ag deposition, the MWNT aerogels were vapor-densified with IPA.

2.3. Synthesis of MWNT aerogels. Free standing MWNT aerogels were drawn from the sidewall of a spinnable MWNT forest synthesized by chemical vapor deposition (CVD)²⁴. The substrates were prepared by depositing 3 nm of iron catalyst using an electron beam (CHA -50) onto Si wafers bearing 100 nm of silicon oxide. A mixture of acetylene (116.8 sccm) and hydrogen (1354 sccm) in a He (2400 sccm) atmosphere were reacted with the substrates at temperatures between 700-730°C for 5-10 min.

2.4. Preparation of the AgNWs/MWNT aerogels. Dry-spun MWNT aerogels were placed on the top of the sheet supports, which had a 1 x 1-inch rectangular aperture in the middle and copper tape electrodes at the edges. Two configurations were prepared: parallel and perpendicular. In the parallel and perpendicular configurations, the MWNT aerogels were placed with the copper electrodes perpendicular to and parallel to the copper electrodes, respectively. Silver paste was painted on top of the contact between the MWNT aerogels and the copper electrodes to ensure sound electrical connection. The sheet resistances, R_s , of the aerogel films were calculated using the formula $R_s = Resistance \left(\frac{MWNT\ aerogel\ length}{MWNT\ aerogel\ width} \right)$. The transmittances of the aerogel for 550-nm-light polarized \perp and \parallel to the MWNT direction were measured using the polarization mode of a UV-Vis spectrometer (Perkin Elmer Lambda 900 UV-Vis/NIR Spectrophotometer).

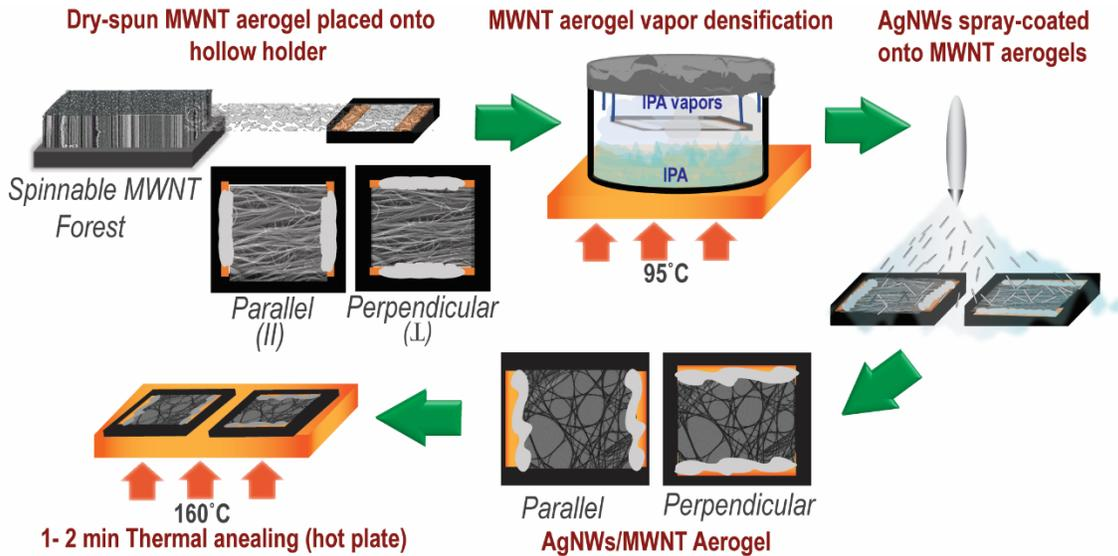


Figure 1. Preparation of flexible AgNWs/MWNTs hybrid TCs

Before spray coating the MWNT aerogels with the AgNW solution, the pristine MWNT aerogels were vapor densified²⁴ using IPA. To accomplish this, 100 mL of IPA was placed in a 500 mL beaker, covered with aluminum foil, and heated on a hot plate at 95°C for 5 minutes to

produce IPA vapors. The aerogels were placed in the beaker (facing down at 2-10 cm distance from the liquid IPA) for 5-30 seconds, and then slowly lifted from the beaker to avoid breakage. A Paasche SI airbrush, which was connected to an Argon or Nitrogen gas source, was used to deposit the AgNWs onto the aerogel at a set pressure of 40 psi. The airbrush was maintained vertically during the entire spray coating process and moved from left to right to ensure uniform coverage of the MWNT aerogel. The distance between the brush nozzle and MWNT aerogels was set at 20-30 cm. Every 20 passes, the sprayed aerogels were placed on a hot plate at 95°C for 5 minutes to complete evaporation of the IPA from the MWNT aerogels. Afterwards, resistance and transmittance measurements were made, as previously described. Thermal annealing at 160°C on a hot plate for 1-2 minutes was performed to decrease the non-effective contacts between AgNWs within the MWNT aerogels and to evaporate any organic solvent residues.

2.5. MWNT aerogel areal density. MWNT aerogel areal density was calculated by dividing the weight of one MWNT aerogel sheet by its area. Using measured weights of 4, 6, 8 and 10 MWNT aerogel sheets, linear regression analysis was used to predict the weight of a single aerogel. The weight of the aerogel sheets was an average of three measurements recorded with a microgram accurate scale. To minimize human error, dimensions of the sheets (width and length) were obtained using an optical microscope with attached camera and analyzed using MatLab to obtain an estimation of the area.

2.6. Physical characterization. AgNWs/MWNTs aerogels morphologies were characterized using scanning electron microscope, SEM (Zeiss-LEO Model 1530 Variable Pressure Field Effect Scanning Electron Microscope).

3. Results and discussion

Figure 2a is a photograph showing the transparency of a AgNWs/MWNTs hybrid TCE that was spray-coated with a 0.25 mg/mL solution of AgNWs and then thermally annealed. This hybrid TCE, which provided $T(\perp) = 98.9\%$ and $R_s(\parallel) = 11 \Omega/\text{sq}$, is self-supporting and can be transferred to a wide range of substrates (glass, polymer, metal, etc.) without the aid of an adhesive layer. Unless otherwise indicated, the AgNWs/MWNTs hybrid TCEs transmittance is perpendicular transmittance, $T(\perp)$, taken at 550nm and the sheet resistance is parallel sheet resistance, $R_s(\parallel)$.

Figure 2b shows the increase in perpendicular transmittance and reduction of parallel sheet resistance, as the amount of deposited AgNWs increases within MWNT aerogels. It highlights the three enhancing mechanisms; Densification Effect, AgNWs Effect and Thermal Annealing Effect, that occur when spray-coating MWNTs aerogels with AgNWs/IPA solution. The first enhancement mechanism, labeled as Densification Effect, is responsible for increasing the AgNWs/MWNTs hybrid TCEs transmittance to values $> 90\%$, and initially reducing the R_s by $\sim 30\%$. Here AgNWs account for a negligible percentage of the total decrease in R_s since a percolated AgNW system has not been achieved³⁰. During this first mechanism, fine droplets of AgNWs/IPA locally wet the MWNT aerogel and IPA surface tension forces develop between parallel MWNTs strands, pushing them into thicker bundles with diameters $\leq 5 \mu\text{m}$. As the IPA solvent evaporates, strong van der Waals forces develop between individual nanotubes within the bundles allowing them to remain collapsed and create apertures greater than wavelength on light ($\lambda_{\text{visible light}}$), Figure 2c. Simultaneously, the $\sim 30\%$ decrease in aerogel's initial R_s occurs when the solvent densifies, or reduces the aerogel initial thickness from $\sim 20 \mu\text{m}$ to $\sim 50 \text{nm}$, creating stronger contacts between individual nanotubes⁶⁵. While the solvent is being evaporated from the MWNT aerogel, AgNWs, carried by the solvent droplets, get deposited on top or between the

newly formed MWNT bundles. A significant reduction of aerogel's R_s is only recorded when AgNWs reached the electrical percolation threshold. At this point, AgNWs have formed enough connecting paths with themselves, other AgNWs and/or with MWNT bundles through which electrons can travel, Figure 2d.

Once the AgNWs electrical percolation threshold is achieved, the second enhancement mechanism, labeled as AgNWs Effect, takes place and the formation of AgNWs conductive network begins. In this zone, solvent densification increases the transmittance $\sim 0.1\%$ while R_s continues to decrease rapidly as more AgNWs get deposited onto the MWNT aerogel, Figure 2e, reaching a maximum of $\sim 70\%$ decrease of the aerogel's R_s after densification effect.

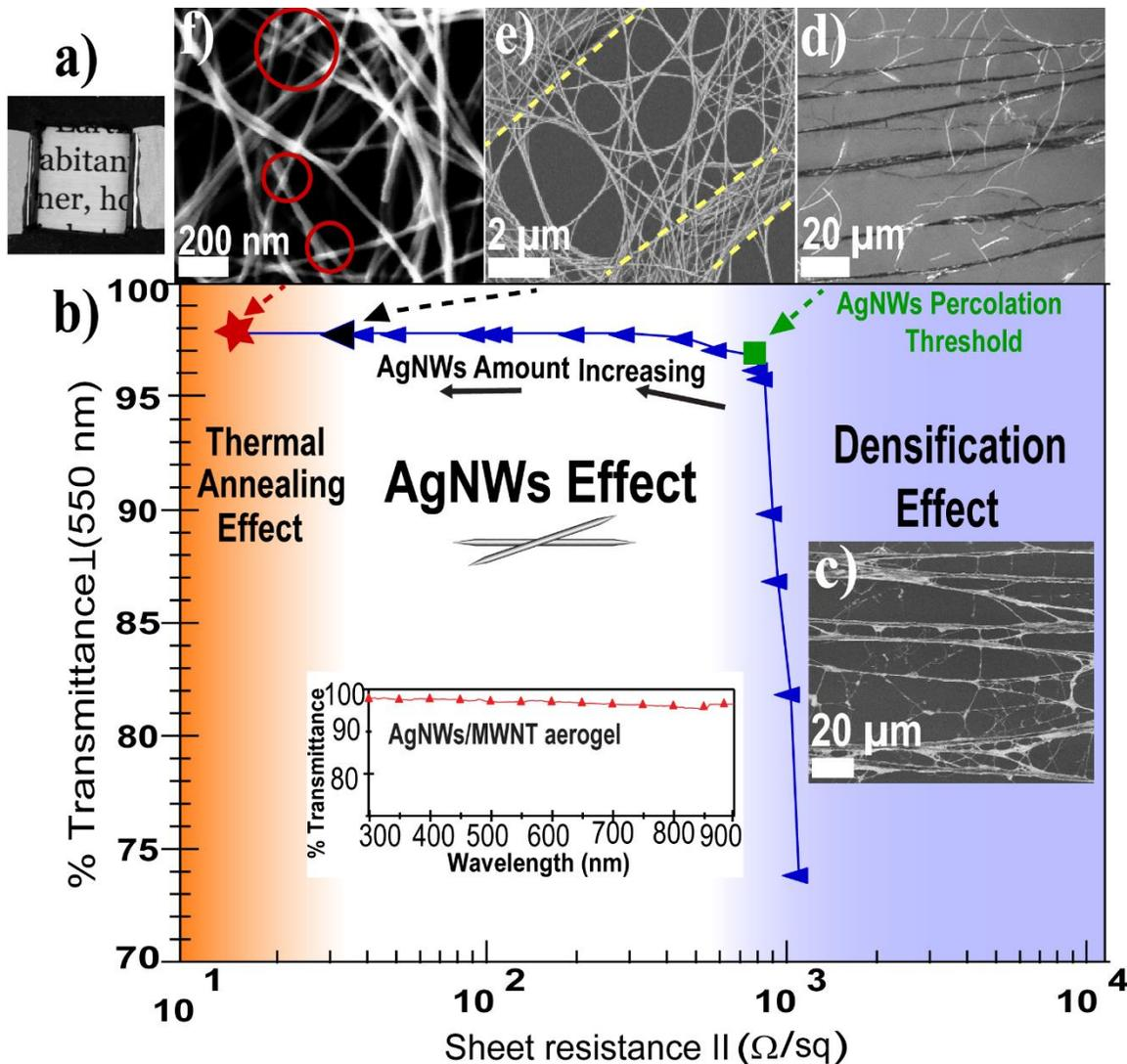


Figure 2. a) AgNWs/MWNTs electrode with $T(\perp) = 98\%$ and $R_s(\parallel) = 11.0\ \Omega/\text{sq}$. b) The three enhancing mechanisms occurring during spray-coating of AgNWs/IPA to MWNTs aerogels; Densification Effect, AgNWs Effect and Thermal Annealing Effect from which the transmittance is increased while the sheet resistance of the AgNWs/MWNT aerogel is reduced. Inset depicts the optical transmittance of the AgNWs/MWNTs hybrids TCE over the visible spectrum. c) SEM image of MWNT aerogel apertures formed as consequence of the densification effect. d) Optical image representing the AgNWs/MWNT aerogel percolation threshold. e) SEM image depicting the AgNWs/MWNT network taken at the lowest sheet resistance achieved before thermal annealing. Dashed lines highlight the contour of MWNT bundles. f) SEM image of AgNWs welded to one another after thermal annealing.

Once the AgNWs conductive network is achieved within the MWNT aerogel, the R_s is further lowered with the third enhancement mechanism; the Thermal Annealing Effect- a one to two-minute thermal annealing process at 160°C . This quick annealing takes advantage of the high thermal conductivity of the MWNTs⁶³ to decrease the non-effective contacts between AgNWs within the MWNT aerogels and evaporates any organic solvent residues from the spray-coating⁵⁴, reducing the R_s of the AgNWs/MWNTs hybrids TCEs by 50%. Figure 2f, show the effectiveness of this quick annealing were the AgNWs welded to one another at each contact point without disrupting the MWNT aerogel. Overheating above the ideal temperature or at prolonged times drastically increases the R_s of the AgNWs/MWNTs TCE hybrids due to the disintegration of AgNWs into Ag droplets, (Figure S1).

Dry-spun MWNT aerogels are anisotropic by nature due to the preferential alignment of nanotubes along the pulling direction. Therefore, it is expected that the optical and electrical

anisotropic behavior of MWNT aerogels also changes when spray-coated with the AgNWs/IPA solution. A suppression of anisotropic polarized transmittance, T_A , along \parallel and \perp nanotube direction, is reduced when $T_A = \parallel/\perp$ quotient is close to unity. From figure 3a, the AgNWs/MWNTs hybrid TCEs behave as a transparent isotropic material when T_A increases from 0.38 to 0.99 as a consequence of MWNT aerogel apertures greater than $\lambda_{\text{visible light}}$ formed during the Densification Effect.

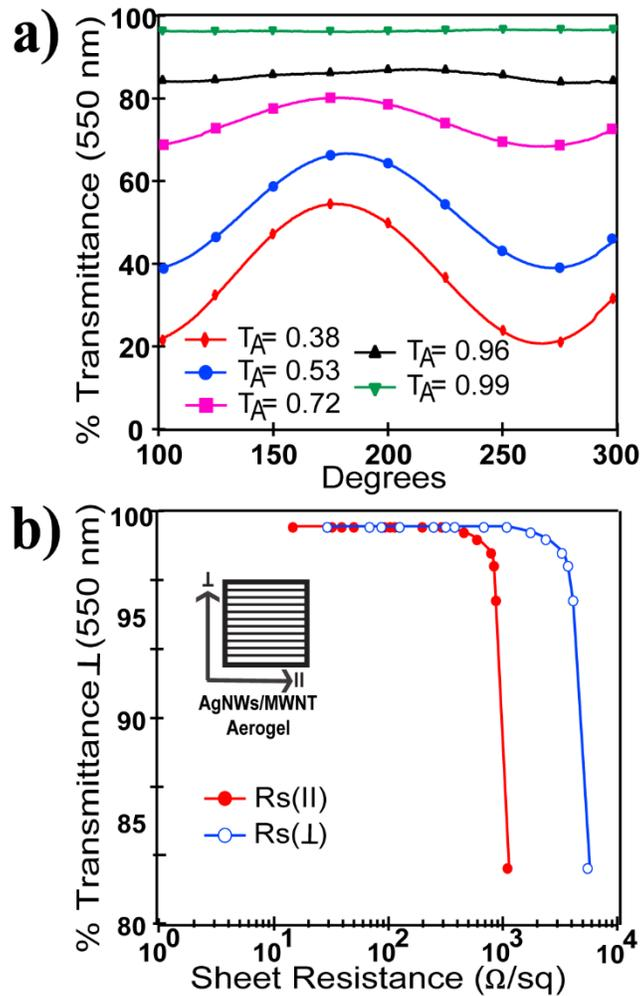


Figure 3. a) Suppression of anisotropic transmittance, T_A , taken at 550 nm while the light source rotated from 100 to 300 degrees. A maximum transmittance is obtained when \vec{E}_{field} is \perp to the MWNTs direction while a minimum is achieved when \vec{E}_{field} is \parallel to the MWNTs

direction. A loss in anisotropic polarization transmittance is achieved when the transmittance anisotropic quotient, $TA = \parallel/\perp$, increased from 0.38 to 0.99, corresponding to the sinusoidal graph profile loss. b) Plot of $T(\perp)$ at 550nm vs R_s in the \parallel and \perp MWNTs direction. The R_s anisotropic behavior, R_{SA} , is reduced when the quotient, $\frac{R_{s(\parallel)}}{R_{s(\perp)}}$, increased from 0.20 to 0.40 corresponding to a final $R_{s(\parallel)} = 11.0 \text{ } \Omega/\text{sq}$ and $R_{s(\perp)} = 29.2 \text{ } \Omega/\text{sq}$, after annealing treatment.

R_s anisotropic behavior, defined as $R_{SA} = \frac{R_{s\parallel}}{R_{s\perp}}$, is reduced when the AgNWs electrical percolation threshold is achieved and continues to be reduced until the AgNW conductive network is established. A R_{SA} quotient close to unity reflects a total loss of anisotropic resistance behavior and represents electrons equally percolating through the AgNWs/MWNT hybrid in the \parallel and \perp MWNT direction. Before spray-coating the MWNT aerogels with the AgNWs/IPA solution, the initial aerogel $R_{s(\perp)}$ is ~ 70 fold higher than $R_{s(\parallel)}$, leading to an $R_{SA} = 0.20$. After spray-coating $0.180 \pm 0.10 \text{ } \mu\text{g}$ of AgNWs, the maximum amount needed to achieve the lowest R_s , a ~ 2.5 fold difference between $R_{s(\perp)}$ and $R_{s(\parallel)}$ is recorded and a $R_{SA} = 0.40$ is achieved, Figure 3b. $R_{s(\perp)}$ is the limiting factor in the R_{SA} equation. For $R_{s(\perp)}$ to have a value similar to $R_{s(\parallel)}$, AgNWs need to connect adjacent MWNTs bundles and arrange a conductive network in the perpendicular direction, requiring AgNWs with lengths \geq MWNT aerogel apertures.

3.2 AgNWs dimension effects

AgNWs length and diameter affect the onset of the AgNWs electrical percolation threshold, the formation of the AgNW conductive network and thus, the overall R_s of the AgNWs/MWNT hybrids TCEs. Figure 4a, plots the transmittance vs R_s of three types of AgNWs with different diameters and lengths spray-coated onto MWNT aerogels. Also shown in this figure is the effect

of spraying exclusively with IPA, outlining the decrease in R_s and increase in transmittance due to densification effect. The highest decrease in R_s is obtained when AgNWs with diameters ~ 22 nm and lengths $\sim 18 \mu\text{m}$ are used, Figure 4a, (blue triangles). These AgNWs are flexible enough that, when sprayed, wrap around individual MWNT bundles, creating more opportunities to connect with itself or with other AgNWs, Figure 4c-d, and long enough to form bridges between adjacent MWNT bundles, properties well suited to create the AgNW conductive network. Effectively, this AgNWs reduce the $R_s \sim 70\%$ after the densification effect.

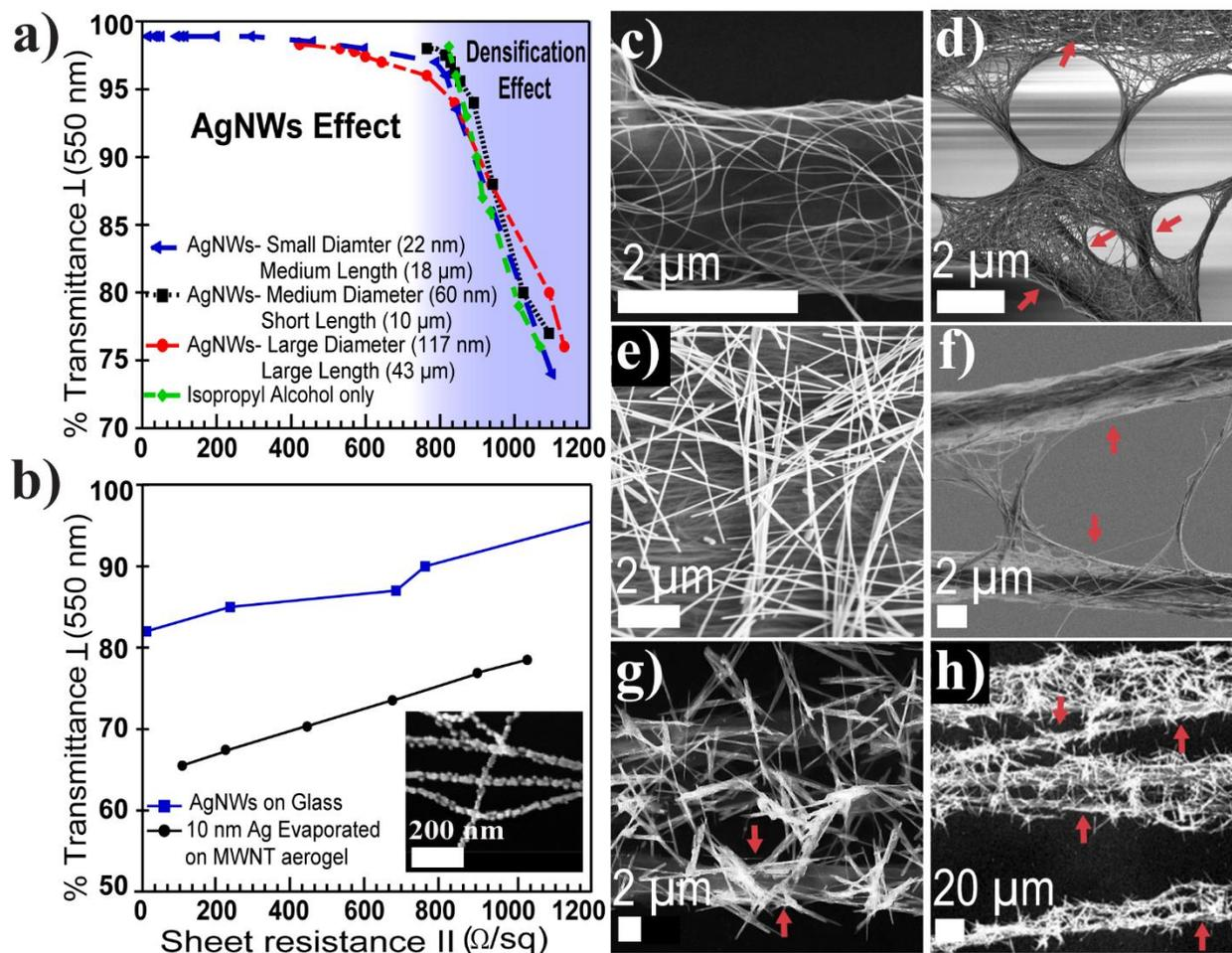


Figure 4. a) Evolution of MWNT aerogels increase in transmittance and decrease in R_s when spray-coated with AgNWs with different diameters and lengths. As a reference, the effect of

spray MWNT aerogels with IPA is also plotted. Linear decrease in transmittance and R_s is seen when b) 10 nm of Ag are e-beam evaporated onto a MWNT aerogel, black circles, or when AgNWs with small diameters (22 nm) and medium lengths (18 μm), are spray-coated to a glass slide, blue squares. Morphology of MWNT aerogel with 10 nm of Ag evaporated is shown as an inset. SEM of c-d) AgNWs with small diameters (22 nm) and medium lengths (18 μm) wrapping and connecting neighbor MWNT bundles, e-f) AgNWs with medium diameters (60 nm) and short lengths (10 μm) laying on top of a MWNT bundle and forming few bridges between adjacent MWNT bundles. g-h) AgNWs with large diameters (117 nm) and large lengths (43 μm) laying between neighbor bundles without wrapping around them. All the SEM images are taken at the lowest R_s achieved before annealing. Arrows indicate MWNT bundles.

On the contrary, AgNWs with diameters ≥ 40 nm and short lengths $< 10\mu\text{m}$, when sprayed to the MWNT aerogels, form non-optimal AgNWs networks and decrease the overall R_s $\sim 10\%$ after densification effect, Figure 4a, black squares. These AgNWs appear to be rigid and lay on top of the MWNT bundles without wrapping around them, forming few bridges between adjacent MWNT when AgNWs agglomeration occur, Figure 4 e-f. If the length of the AgNWs is $\geq 18 \mu\text{m}$ and the diameter ≥ 40 nm is maintained, a 50% decrease in R_s is seen after densification effect, Figure 4a, red circles. In this case, AgNWs interconnect neighboring MWNT bundles, without wrapping around them, Figure 4 g-f.

Transmittance can still attain high values disregarding the type of AgNWs sprayed onto the MWNT aerogel since it is a process affected solely by MWNT aerogel's solvent densification and independent of AgNWs dimension. The inverse proportionality between transmittance and R_s , is only observed when MWNT aerogels are sprayed-coated with an AgNWs/IPA solution, and not when silver is evaporated onto MWNT aerogels or when AgNWs/IPA are spray-coated

to glass slides. Silver evaporated onto a MWNT aerogel is a solvent-free technique and spray-coating AgNWs to glass is unaffected by densification mechanisms thus, transmittance and R_s decrease linearly as the amount of deposited silver increases, Figure 4b.

3.3. MWNTs aerogel density effect

MWNT aerogel density plays an important role in constraining the maximum transmittance and minimum R_s , in the \perp and \parallel direction, that the AgNWs/MWNTs hybrids can reach. Ideally, low AgNWs network densities are desired to reduce optical haze of the hybrid TCEs and still obtain low R_s and high transmittances³⁰. Though long and thin AgNWs are required to form ideal AgNWs conductive networks necessary to lower the R_s , MWNT aerogel areal density limits the amount of AgNWs per unit area needed to reach the lowest R_s and highest transmittance. Aerogels with high areal densities $\sim 5.6 \mu\text{g}/\text{cm}^2$, have initial low transmittances, $T = 53 \pm 5\%$ and not to high sheet resistances, $R_s = 410 \pm 25 \Omega/\text{sq}$. These aerogels require a low AgNWs mass density of $\sim 20.6 \mu\text{g}/\text{cm}^2$ to obtain a $R_s \sim 10 \Omega/\text{sq}$ after annealing, with final $T \sim 90\%$. For MWNT aerogels with low areal densities $\sim 2.8 \mu\text{g}/\text{cm}^2$, the initial R_s and transmittances are $825 \pm 50 \Omega/\text{sq}$ and $70 \pm 10\%$, respectively. With a AgNWs mass density of $\sim 50.0 \mu\text{g}/\text{cm}^2$, these MWNT aerogels can achieve $R_s \sim 11 \Omega/\text{sq}$ after annealing; values similar to MWNT aerogels with high areal density, but on the contrary, transmittances as high as 99% can be achieved, Figure 5.

A tradeoff between MWNT aerogel areal density and AgNWs mass density exist that greatly influence the optical and electrical properties of the AgNWs/MWNTs hybrid TCEs. Since low MWNT aerogel areal densities have less CNTs/ cm^2 , when densified with the AgNWs/IPA solution, thinner bundles and bigger apertures are formed allowing the transmittance to achieve values $>90\%$. The lower $< 90\%$ transmittance, seen in MWNT aerogels with high areal densities

is a consequence of more carbon nanotubes/cm² available to form additional and/or thicker MWNT bundles when densified, creating apertures lower than the λ_{light} that absorb or reflect the incident light more efficiently.

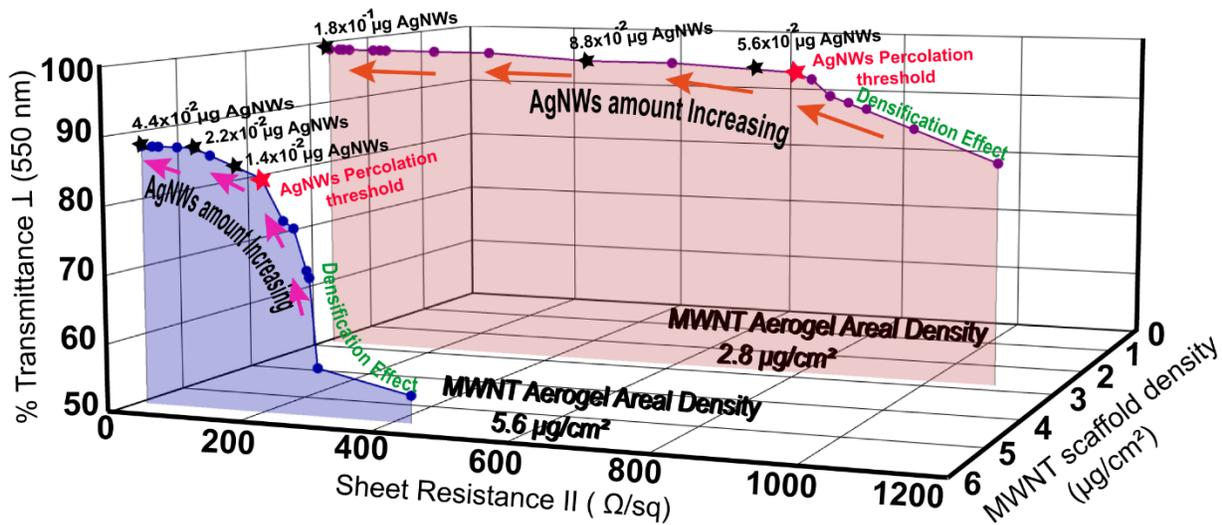


Figure 5. Transmittance I (550 nm) vs sheet resistance II plotted as a function of MWNT aerogel areal density.

4. Conclusion

In this study hybrid and self-supported TCEs made of AgNWs spray-coated onto MWNTs aerogels have proven to achieve simultaneous increase in transmittances above 90% and decrease in Rs below 15 Ω/sq by in situ formation of MWNT aerogel apertures and deposition of AgNWs. AgNWs with small diameters (22 nm) and medium lengths (18 μm) were found to create ideal AgNWs conductive networks when spray-coated to MWNT aerogels by wrapping around MWNT bundles, creating effective connections with themselves and with neighbor MWNT bundles. MWNT aerogel Rs and transmittance anisotropic behavior was also suppressed by the formation of apertures with sizes larger than the wavelength of light and by creating new electrical pathways when AgNWs connected neighbor MWNT bundles. The reduced electrical

anisotropy is desired for many applications in optoelectronics where charge injection or collection from the transparent electrode is expected to be uniform and isotropic in all direction.

MWNT aerogel with areal densities similar or below $2.8 \mu\text{g}/\text{cm}^2$, were found to be the most suitable aerogels for AgNWs deposition due to their intrinsic high transmittance. However, the high sheet resistance of these low-density aerogels required a greater amount of AgNWs $\sim 50 \mu\text{g}/\text{cm}^2$ to achieve low Rs. Of great interest is the ability to fine tune the amount of AgNWs needed within the MWNT aerogel for achieving the percolation critical point. This suggest further research in achieving an optimal balance of AgNWs and MWNTs possible to maximize the desirable properties of this system as a new form of TCE. What more, these materials can be easily transferred onto various substrates, making them applicable to a wide variety of technologies within the flexible electronics community, allowing for applications not possible with traditional TCEs currently available.

AUTHOR INFORMATION

Corresponding Author

* Corresponding author. Tel: 972-883-6218. Email: zakhidov@utdallas.edu (Anvar Zakhidov)

Present Addresses

† California Institute of Technology, 1200 East California Boulevard, Pasadena, California 91125, United States.

Author Contributions

All authors have given approval to the final version of the manuscript.

Funding Sources

Partial financial support from the Ministry of Education and Science of the Russian Federation (Grant № 14.Y26.31.0010 for optical measurements) and grant in the framework of Increase

Competitiveness Program of NUST “MISiS” (No. K2-2015-014 for samples preparation) is acknowledged. Also, a support of Welch Foundation of Texas via grant AT-1617 and Navy STTR Marcorp N181-002-1004 is highly appreciated.

ACKNOWLEDGEMENTS

Patricia M. Martinez would like to acknowledge CONACYT and the Mexican government for academic opportunities and support.

ABBREVIATIONS

ITO, Indium Thin Oxide; TCEs, Transparent Conducting Electrodes; MWNTs, Multiwall Carbon Nanotube; AgNWs, silver nanowires; Rs, sheet resistance; T, Transmittance; CVD, Chemical Vapor Deposition.

REFERENCES

- (1) Lin, H. K.; Hsu, W. C. Electrode Patterning of ITO Thin Films by High Repetition Rate Fiber Laser. *Appl. Surf. Sci.* **2014**, *308*, 58–62.
- (2) Alzoubi, K.; Hamasha, M. M.; Lu, S.; Sammakia, B. Bending Fatigue Study of Sputtered ITO on Flexible Substrate. *J. Disp. Technol.* **2011**, *7* (11), 593–600.
- (3) Peng, L.; Feng, Y.; Lv, P.; Lei, D.; Shen, Y.; Li, Y.; Feng, W. Transparent, Conductive, and Flexible Multiwalled Carbon Nanotube/Graphene Hybrid Electrodes with Two Three-Dimensional Microstructures. *J. Phys. Chem. C* **2012**, *116* (8), 4970–4978.
- (4) Dattoli, E. N.; Lu, W. ITO Nanowires and Nanoparticles for Transparent Films. *MRS Bull.* **2011**, *36* (10), 782–788.

- (5) Sakamoto, K.; Kuwae, H.; Kobayashi, N.; Nobori, A.; Shoji, S.; Mizuno, J. Highly Flexible Transparent Electrodes Based on Mesh-Patterned Rigid Indium Tin Oxide. *Sci. Rep.* **2018**, *8* (1), 2825.
- (6) Zhou, Y.; Azumi, R. Carbon Nanotube Based Transparent Conductive Films: Progress, Challenges, and Perspectives. *Science and Technology of Advanced Materials*. 2016, pp 493–516.
- (7) Sun, J.; Wang, R. Carbon Nanotube Transparent Electrode. In *Syntheses and Applications of Carbon Nanotubes and Their Composites*; 2013.
- (8) Aloui, W.; Ltaief, A.; Bouazizi, A. Transparent and Conductive Multi Walled Carbon Nanotubes Flexible Electrodes for Optoelectronic Applications. *Superlattices Microstruct.* **2013**, *64*, 581–589.
- (9) Jiang, S.; Hou, P. X.; Chen, M. L.; Wang, B. W.; Sun, D. M.; Tang, D. M.; Jin, Q.; Guo, Q. X.; Zhang, D. D.; Du, J. H.; et al. Ultrahigh-Performance Transparent Conductive Films of Carbon-Welded Isolated Single-Wall Carbon Nanotubes. *Sci. Adv.* **2018**, *4* (5), eaap9264.
- (10) Hecht, D. S.; Hu, L.; Irvin, G. Emerging Transparent Electrodes Based on Thin Films of Carbon Nanotubes, Graphene, and Metallic Nanostructures. *Advanced Materials*. Wiley-Blackwell April 5, 2011, pp 1482–1513.
- (11) Doherty, E. M.; De, S.; Lyons, P. E.; Shmeliov, A.; Nirmalraj, P. N.; Scardaci, V.; Joimel, J.; Blau, W. J.; Boland, J. J.; Coleman, J. N. The Spatial Uniformity and Electromechanical Stability of Transparent, Conductive Films of Single Walled Nanotubes. *Carbon N. Y.* **2009**, *47* (10), 2466–2473.

(12) Tenent, R. C.; Barnes, T. M.; Bergeson, J. D.; Ferguson, A. J.; To, B.; Gedvilas, L. M.; Heben, M. J.; Blackburn, J. L. Ultrasoother, Large-Area, High-Uniformity, Conductive Transparent Single-Walled-Carbon-Nanotube Films for Photovoltaics Produced by Ultrasonic Spraying. *Adv. Mater.* **2009**, *21* (31), 3210–3216.

(13) Hu, L.; Hecht, D. S.; Gruner, G. Percolation in Transparent and Conducting Carbon Nanotube Networks. *Nano Lett.* **2004**, *4* (12), 2513–2517.

(14) Blackburn, J. L.; Barnes, T. M.; Beard, M. C.; Kim, Y. H.; Tenent, R. C.; McDonald, T. J.; To, B.; Coutts, T. J.; Heben, M. J. Transparent Conductive Single-Walled Carbon Nanotube Networks with Precisely Tunable Ratios of Semiconducting and Metallic Nanotubes. *ACS Nano* **2008**, *2* (6), 1266–1274.

(15) Wu, Z.; Chen, Z.; Du, X.; Logan, J. M.; Sippel, J.; Nikolou, M.; Kamaras, K.; Reynolds, J. R.; Tanner, D. B.; Hebard, A. F.; et al. Transparent, Conductive Carbon Nanotube Films. *Science (80-.)*. **2004**, *305* (5688), 1273–1276.

(16) Tokuno, T.; Nogi, M.; Jiu, J.; Suganuma, K. Hybrid Transparent Electrodes of Silver Nanowires and Carbon Nanotubes: A Low-Temperature Solution Process. *Nanoscale Res. Lett.* **2012**, *7* (1), 281.

(17) Wassei, J. K.; Kaner, R. B. Graphene, a Promising Transparent Conductor. *Materials Today*. Elsevier March 1, 2010, pp 52–59.

(18) Tung, V. C.; Allen, M. J.; Yang, Y.; Kaner, R. B. High-Throughput Solution Processing of Large-Scale Graphene. *Nat. Nanotechnol.* **2009**, *4* (1), 25–29.

- (19) Wang, X.; Zhi, L.; Müllen, K. Transparent, Conductive Graphene Electrodes for Dye-Sensitized Solar Cells. *Nano Lett.* **2008**, *8* (1), 323–327.
- (20) Eda, G.; Fanchini, G.; Chhowalla, M. Large-Area Ultrathin Films of Reduced Graphene Oxide as a Transparent and Flexible Electronic Material. *Nat. Nanotechnol.* **2008**, *3* (5), 270–274.
- (21) Jurewicz, I.; Fahimi, A.; Lyons, P. E.; Smith, R. J.; Cann, M.; Large, M. L.; Tian, M.; Coleman, J. N.; Dalton, A. B. Insulator-Conductor Type Transitions in Graphene-Modified Silver Nanowire Networks: A Route to Inexpensive Transparent Conductors. *Adv. Funct. Mater.* **2014**, *24* (48), 7580–7587.
- (22) Hecht, D. S.; Hu, L.; Irvin, G. Emerging Transparent Electrodes Based on Thin Films of Carbon Nanotubes, Graphene, and Metallic Nanostructures. *Adv. Mater.* **2011**, *23* (13), 1482–1513.
- (23) Kholmanov, I. N.; Magnuson, C. W.; Piner, R.; Kim, J. Y.; Aliev, A. E.; Tan, C.; Kim, T. Y.; Zakhidov, A. A.; Sberveglieri, G.; Baughman, R. H.; et al. Optical, Electrical, and Electromechanical Properties of Hybrid Graphene/Carbon Nanotube Films. *Adv. Mater.* **2015**, *27* (19), 3053–3059.
- (24) Zhang, M.; Fang, S.; Zakhidov, A. A.; Lee, S. B.; Aliev, A. E.; Williams, C. D.; Atkinson, K. R.; Baughman, R. H. Strong, Transparent, Multifunctional, Carbon Nanotube Sheets. *Science (80-.).* **2005**, *309* (5738), 1215–1219.

- (25) Luo, M.; Liu, Y.; Huang, W.; Qiao, W.; Zhou, Y.; Ye, Y.; Chen, L. Sen. Towards Flexible Transparent Electrodes Based on Carbon and Metallic Materials. *Micromachines*. Multidisciplinary Digital Publishing Institute January 4, 2017, p 12.
- (26) Ackermann, T.; Neuhaus, R.; Roth, S. The Effect of Rod Orientation on Electrical Anisotropy in Silver Nanowire Networks for Ultra-Transparent Electrodes. *Sci. Rep.* **2016**, *6*, 34289.
- (27) Lagrange, M.; Langley, D. P.; Giusti, G.; Jiménez, C.; Bréchet, Y.; Bellet, D. Optimization of Silver Nanowire-Based Transparent Electrodes: Effects of Density, Size and Thermal Annealing. *Nanoscale* **2015**, *7* (41), 17410–17423.
- (28) Liang, J.; Li, L.; Tong, K.; Ren, Z.; Hu, W.; Niu, X.; Chen, Y.; Pei, Q. Silver Nanowire Percolation Network Soldered with Graphene Oxide at Room Temperature and Its Application for Fully Stretchable Polymer Light-Emitting Diodes. *ACS Nano* **2014**, *8* (2), 1590–1600.
- (29) Ricciardulli, A. G.; Yang, S.; Wetzelaer, G.-J. J. A. H.; Feng, X.; Blom, P. W. M. Hybrid Silver Nanowire and Graphene-Based Solution-Processed Transparent Electrode for Organic Optoelectronics. *Adv. Funct. Mater.* **2018**, *28* (14), 1706010.
- (30) Langley, D. Silver Nanowire Networks : Effects of Percolation and Thermal Annealing on Physical Properties, 2014.
- (31) Bellet, D.; Lagrange, M.; Sannicolo, T.; Aghazadehchors, S.; Nguyen, V. H.; Langley, D. P.; Muñoz-Rojas, D.; Jiménez, C.; Bréchet, Y.; Nguyen, N. D. Transparent Electrodes Based on Silver Nanowire Networks: From Physical Considerations towards Device Integration. *Materials (Basel)*. **2017**, *10* (6).

- (32) Lee, J. Y.; Connor, S. T.; Cui, Y.; Peumans, P. Solution-Processed Metal Nanowire Mesh Transparent Electrodes. *Nano Lett.* **2008**, *8* (2), 689–692.
- (33) De, S.; Higgins, T. M.; Lyons, P. E.; Doherty, E. M.; Nirmalraj, P. N.; Blau, W. J.; Boland, J. J.; Coleman, J. N. Silver Nanowire Networks as Flexible, Transparent, Conducting Films: Extremely High DC to Optical Conductivity Ratios. *ACS Nano* **2009**, *3* (7), 1767–1774.
- (34) Hu, L.; Kim, H. S.; Lee, J. Y.; Peumans, P.; Cui, Y. Scalable Coating and Properties of Transparent, Flexible, Silver Nanowire Electrodes. *ACS Nano* **2010**, *4* (5), 2955–2963.
- (35) Zhu, R.; Chung, C. H.; Cha, K. C.; Yang, W.; Zheng, Y. B.; Zhou, H.; Song, T. Bin; Chen, C. C.; Weiss, P. S.; Li, G.; et al. Fused Silver Nanowires with Metal Oxide Nanoparticles and Organic Polymers for Highly Transparent Conductors. *ACS Nano* **2011**, *5* (12), 9877–9882.
- (36) Garnett, E. C.; Cai, W.; Cha, J. J.; Mahmood, F.; Connor, S. T.; Greyson Christoforo, M.; Cui, Y.; McGehee, M. D.; Brongersma, M. L. Self-Limited Plasmonic Welding of Silver Nanowire Junctions. *Nat. Mater.* **2012**, *11* (3), 241–249.
- (37) Maisch, P.; Tam, K. C.; Lucera, L.; Egelhaaf, H. J.; Scheiber, H.; Maier, E.; Brabec, C. J. Inkjet Printed Silver Nanowire Percolation Networks as Electrodes for Highly Efficient Semitransparent Organic Solar Cells. *Org. Electron. physics, Mater. Appl.* **2016**, *38*, 139–143.
- (38) Tokuno, T.; Nogi, M.; Karakawa, M.; Jiu, J.; Nge, T. T.; Aso, Y.; Suganuma, K. Fabrication of Silver Nanowire Transparent Electrodes at Room Temperature. *Nano Res.* **2011**, *4* (12), 1215–1222.

- (39) Madaria, A. R.; Kumar, A.; Zhou, C. Large Scale, Highly Conductive and Patterned Transparent Films of Silver Nanowires on Arbitrary Substrates and Their Application in Touch Screens. *Nanotechnology* **2011**, *22* (24), 245201.
- (40) Yu, Z.; Zhang, Q.; Li, L.; Chen, Q.; Niu, X.; Liu, J.; Pei, Q. Highly Flexible Silver Nanowire Electrodes for Shape-Memory Polymer Light-Emitting Diodes. *Adv. Mater.* **2011**, *23* (5), 664–668.
- (41) Zeng, X. Y.; Zhang, Q. K.; Yu, R. M.; Lu, C. Z. A New Transparent Conductor: Silver Nanowire Film Buried at the Surface of a Transparent Polymer. *Adv. Mater.* **2010**, *22* (40), 4484–4488.
- (42) Gaynor, W.; Burkhard, G. F.; McGehee, M. D.; Peumans, P. Smooth Nanowire/Polymer Composite Transparent Electrodes. *Adv. Mater.* **2011**, *23* (26), 2905–2910.
- (43) Lee, J. Y.; Connor, S. T.; Cui, Y.; Peumans, P. Semitransparent Organic Photovoltaic Cells with Laminated Top Electrode. *Nano Lett.* **2010**, *10* (4), 1276–1279.
- (44) Gaynor, W.; Lee, J. Y.; Peumans, P. Fully Solution-Processed Inverted Polymer Solar Cells with Laminated Nanowire Electrodes. *ACS Nano* **2010**, *4* (1), 30–34.
- (45) Madaria, A. R.; Kumar, A.; Ishikawa, F. N.; Zhou, C. Uniform, Highly Conductive, and Patterned Transparent Films of a Percolating Silver Nanowire Network on Rigid and Flexible Substrates Using a Dry Transfer Technique. *Nano Res.* **2010**, *3* (8), 564–573.
- (46) Scardaci, V.; Coull, R.; Lyons, P. E.; Rickard, D.; Coleman, J. N. Spray Deposition of Highly Transparent, Low-Resistance Networks of Silver Nanowires over Large Areas. *Small* **2011**, *7* (18), 2621–2628.

(47) Naito, K.; Inuzuka, R.; Yoshinaga, N.; Mei, W. Transparent Conducting Films Composed of Graphene Oxide/Ag Nanowire/ Graphene Oxide/PET. *Synth. Met.* **2018**, *237*, 50–55.

(48) Miao, J.; Chen, S.; Liu, H.; Zhang, X. Low-Temperature Nanowelding Ultrathin Silver Nanowire Sandwiched between Polydopamine-Functionalized Graphene and Conjugated Polymer for Highly Stable and Flexible Transparent Electrodes. *Chem. Eng. J.* **2018**, *345*, 260–270.

(49) Liu, J.; Jiang, T.; Duan, F.; Shen, G.; He, X.; Yang, W.; Liang, P.; Yue, Y.; Lan, Q.; Wu, J.; et al. Electrophoresis Deposition of Flexible and Transparent Silver Nanowire/Graphene Composite Film and Its Electrochemical Properties. *J. Alloys Compd.* **2018**, *745*, 370–377.

(50) Chung, W. H.; Park, S. H.; Joo, S. J.; Kim, H. S. UV-Assisted Flash Light Welding Process to Fabricate Silver Nanowire/Graphene on a PET Substrate for Transparent Electrodes. *Nano Res.* **2018**, *11* (4), 2190–2203.

(51) Ricciardulli, A. G.; Yang, S.; Wetzelaer, G. J. A. H.; Feng, X.; Blom, P. W. M. Hybrid Silver Nanowire and Graphene-Based Solution-Processed Transparent Electrode for Organic Optoelectronics. *Adv. Funct. Mater.* **2018**, *28* (14).

(52) Lee, C.; Oh, Y.; Yoon, I. S.; Kim, S. H.; Ju, B.-K.; Hong, J.-M. Flash-Induced Nanowelding of Silver Nanowire Networks for Transparent Stretchable Electrochromic Devices. *Sci. Rep.* **2018**, *8* (1), 2763.

(53) Radmilović, V. V.; Göbel, M.; Ophus, C.; Christiansen, S.; Spiecker, E.; Radmilović, V. R. Low Temperature Solid-State Wetting and Formation of Nanowelds in Silver Nanowires. *Nanotechnology* **2017**, *28* (38), 385701.

(54) Langley, D. P.; Lagrange, M.; Giusti, G.; Jiménez, C.; Bréchet, Y.; Nguyen, N. D.; Bellet, D. Metallic Nanowire Networks: Effects of Thermal Annealing on Electrical Resistance. *Nanoscale* **2014**, *6*.

(55) Jing, M. xiang; Han, C.; Li, M.; Shen, X. qian. High Performance of Carbon Nanotubes/Silver Nanowires-PET Hybrid Flexible Transparent Conductive Films via Facile Pressing-Transfer Technique. *Nanoscale Res. Lett.* **2014**, *9* (1), 588.

(56) Pillai, S. K. R.; Wang, J.; Wang, Y.; Sk, M. M.; Prakoso, A. B.; Rusli; Chan-Park, M. B. Totally Embedded Hybrid Thin Films of Carbon Nanotubes and Silver Nanowires as Flat Homogenous Flexible Transparent Conductors. *Sci. Rep.* **2016**, *6* (1), 38453.

(57) Lee, C.; Oh, Y.; Yoon, I. S.; Kim, S. H.; Ju, B.-K.; Hong, J.-M. Flash-Induced Nanowelding of Silver Nanowire Networks for Transparent Stretchable Electrochromic Devices. *Sci. Rep.* **2018**, *8* (1), 2763.

(58) Li, J.; Tao, Y.; Chen, S.; Li, H.; Chen, P.; Wei, M. Z.; Wang, H.; Li, K.; Mazzeo, M.; Duan, Y. A Flexible Plasma-Treated Silver-Nanowire Electrode for Organic Light-Emitting Devices. *Sci. Rep.* **2017**, *7* (1), 16468.

(59) Lee, H. J.; Oh, S.; Cho, K. Y.; Jeong, W. L.; Lee, D. S.; Park, S. J. Spontaneous and Selective Nanowelding of Silver Nanowires by Electrochemical Ostwald Ripening and High Electrostatic Potential at the Junctions for High-Performance Stretchable Transparent Electrodes. *ACS Appl. Mater. Interfaces* **2018**, *10* (16), 14124–14131.

(60) Huang, Y.; Bai, X.; Zhou, M.; Liao, S.; Yu, Z.; Wang, Y.; Wu, H. Large-Scale Spinning of Silver Nanofibers as Flexible and Reliable Conductors. *Nano Lett.* **2016**, *16* (9), 5846–5851.

(61) Chen, J.; Guo, Y.; Huang, L.; Xue, Y.; Geng, D.; Liu, H.; Wu, B.; Yu, G.; Hu, W.; Liu, Y.; et al. Controllable Fabrication of Ultrathin Free-Standing Graphene Films. *Philos. Trans. R. Soc. A Math. Phys. Eng. Sci.* **2014**, *372* (2013), 20130017.

(62) Liu, Q.; Fujigaya, T.; Cheng, H. M.; Nakashima, N. Free-Standing Highly Conductive Transparent Ultrathin Single-Walled Carbon Nanotube Films. *J. Am. Chem. Soc.* **2010**, *132* (46), 16581–16586.

(63) Aliev, A. E.; Guthy, C.; Zhang, M.; Fang, S.; Zakhidov, A. A.; Fischer, J. E.; Baughman, R. H. Thermal Transport in MWCNT Sheets and Yarns. *Carbon N. Y.* **2007**, *45* (15), 2880–2888.

(64) Vinogradov, V. V.; Felner, I.; Nowik, I.; Avnir, D. Conductive Magnetic Sol-Gel Films. *J. Mater. Chem. C* **2015**, *3* (41), 10723–10727.

(65) Zhang, M.; Fang, S.; Zakhidov, A. A.; Lee, S. B.; Aliev, A. E.; Williams, C. D.; Atkinson, K. R.; Baughman, R. H. Strong, Transparent, Multifunctional, Carbon Nanotube Sheets. *Science (80-.)*. **2005**, *309* (5738).

(66) L. Hu; D. S. Hecht, and; Grüner*, G. Percolation in Transparent and Conducting Carbon Nanotube Networks. **2004**.

Supplementary information

Thermal annealing at temperatures > 160 °C causes the disintegration of AgNWs that connect MWNT bundles and only the AgNWs deposited on top of MWNT bundles suffer a droplet formation, shown in Figure S1. As a consequence, an increase in $R_s(\parallel)$ is recorded without affecting the $T(\perp)$ at 550 nm.

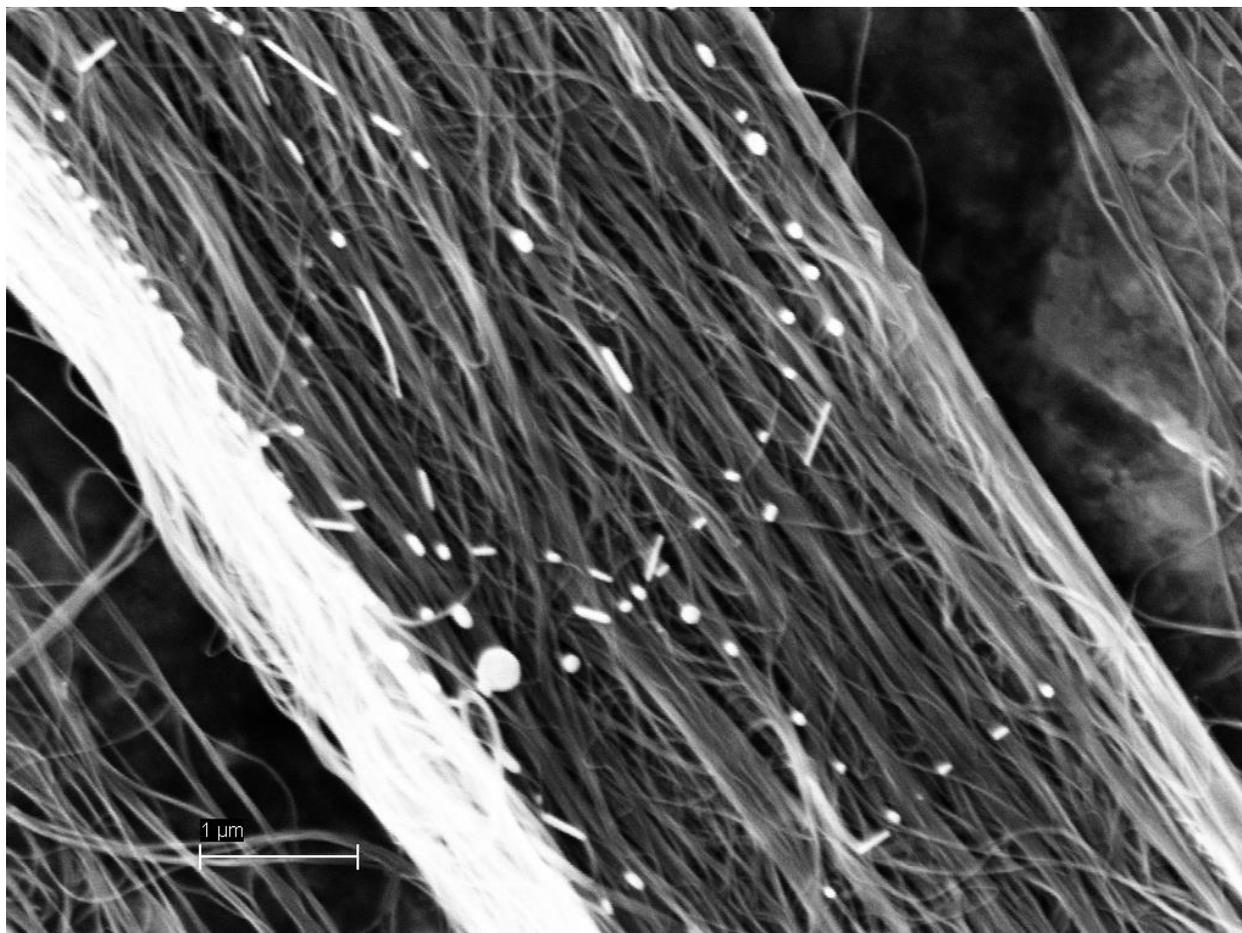


Figure S3. AgNWs disintegrate into droplets after thermal annealing treatment at 200°C.